Energy and Angular Distribution of Electrons ejected from Autoionization States in Helium by Electron Impact

AUTHOR(S):

Tahira, Sadamu

CITATION:

Tahira, Sadamu. Energy and Angular Distribution of Electrons ejected from Autoionization States in Helium by Electron Impact. Memoirs of the Faculty of Science, Kyoto University. Series of physics, astrophysics, geophysics and chemistry 1972, 34(1): 1-28

ISSUE DATE:

1972-12

URL:

http://hdl.handle.net/2433/257525

Memoirs of the Faculty of Science, Kyoto University, Series of Physics, Astrophysics, Geophysics and Chemistry, Vol. XXXIV, No. 1. Article 1, 1972.

ENERGY AND ANGULAR DISTRIBUTION OF ELECTRONS EJECTED FROM AUTOIONIZATION STATES IN HELIUM BY ELECTRON IMPACT*

BY

Sadamu TAHIRA

Department of Physics, Faculty of Science, Kyoto University

(Received February 19, 1971)

ABSTRACT

Energy spectra of electrons ejected from autoionization states in helium excited by electron impact were measured at bombarding energies from 65 to 1000 eV as a function of the ejection angle to the primary electron beam. The measurements of the energy spectra over the wide energy range of autoionized electrons were performed with an energy resolution of 0.15 eV in FWHM, whereas the details of the spectra within a narrow energy range were measured with better resolution, i.e. 0.08 eV in FWHM. The excitation energies of twelve autoionization states in helium were obtained. The line shape of the energy spectra due to autoionized electrons undergoes a marked change with ejection angle. The peaks due to $(2p^2)^1D$ state and those due to $(2s2p)^1P$ state are completely separated in the forward direction. The peak energy of $(2p^2)^1D$ state is 59.89-eV in the forward direction and 59.92-eV in the backward direction. The resonance peak height of $(2s2p)^3P$ state is most prominent when the energy of primary electrons approaches to the excitation energy of this state. Some of the energy spectra due to autoionized electrons were analyzed utilizing the Fano's configuration interaction theory and the applicability of this theory to the present experimental results were confirmed.

1. Introduction

Although the ionization processes induced by the electron impact have been investigated experimentally as well as theoretically for many years, most of these studies have been directed towards the study on the total ionization cross sections[2] and very few information has been available on the energy and angular distribution of secondary electrons, that is electrons resulting from the ionizing collision of the electrons with atoms and molecules.

The energy spectrum of electrons resulting from the collisions of electrons with atoms in an certain direction is shown schematically in Fig. 1. The energy level diagram corresponding to the ionization processes in helium by electron impact is shown in Fig. 2. In Figs. 1 and 2, E_0 and I_0 are the energy of incident electrons and the first ionization potential of atoms, respectively. An electron of energy, E_0, collides with an atom and loses energy amounting to E_3+I_0 in a direct ionizing collision, where E_3 is the energy of electron ejected from atom. The energy of the scattered electron is E_4. The values of E_3 and E_4 can be varied continuously, following to the law of the energy conservation,

$$E_0=E_3+E_4+I_0\,. \tag{1}$$

* A part of this paper was published in Physical Review Letters[1]

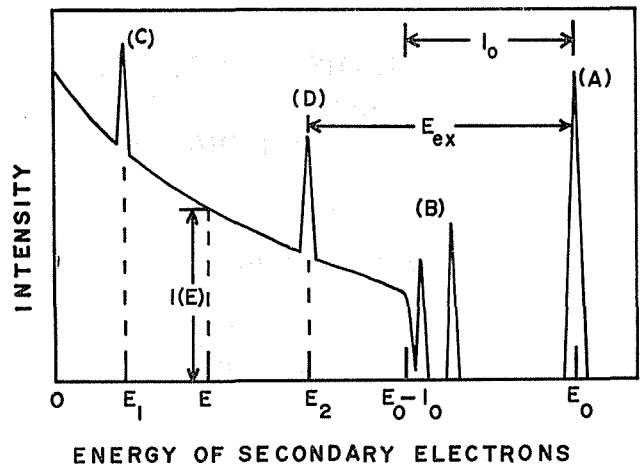

Fig. 1. Schematic energy spectrum due to secondary electrons resulting from ionizing collisions of electrons with atoms, where E_0 and I_0 mean the energy of incident electons and the first ionization potential of atoms, respectively.
A. electrons scattered elastically by atoms, B. electrons scattered inelastically by atoms after exciting singly excited states, D. electrons scattered inelastically by atoms after exciting autoionization state, C. electrons ejected from autoionization state.

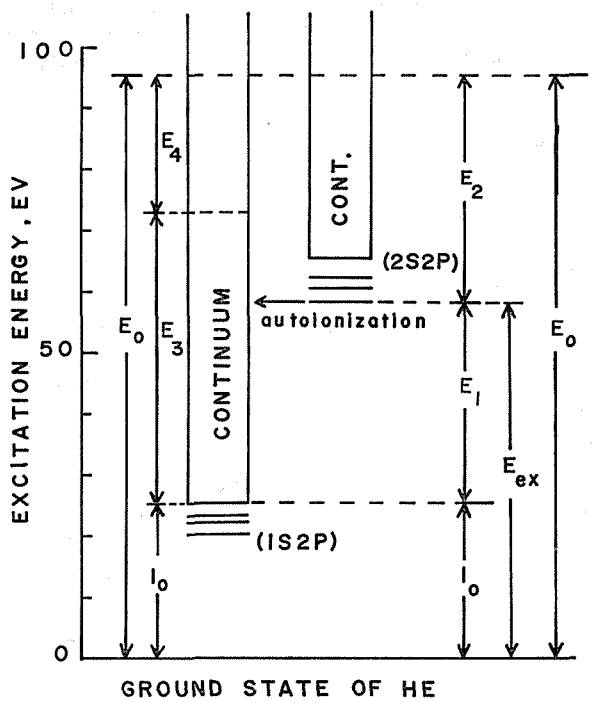

Fig. 2. Energy level diagram of helium, representing the direct and indirect ionization processes by electron impact.

In Fig. 1, the continuum spectrum in the energy region from zero to E_0-I_0 is due to the direct ionization of atoms by electron impact. The intensity, $I(E)$, at an certain energy, E, in this energy region is the sum of intensity due to electrons ejected from atoms and that due to electrons scattered by atoms.

The ionization by electron impact can be classified into two groups, i.e. the direct ionization process, which was mentioned above, and the indirect ionization process. The autoionization process in helium, which is a typical example of the indirect ionization, is shown at the right hand-side of Fig. 2, in which the doubly excited state excited by the primary electron with an energy of E_0 autoionizes into the continuum state and an electron is ejected with the energy of E_1. The value of the energy, E_1, is determined by

$$E_1=E_{ex}-I_0\,, \tag{2}$$

where E_{ex} is the excitation energy of the doubly excited state. The electrons ejected from the autoionization states have the discrete energy independent of the primary energy, E_0, and are observed as the sharp line spectra superimposed upon the continuum such as (C) shown in Fig. 1. The line spectrum, (D), shown in Fig. 2 is due to the electrons scattered inelastically with energy of E_2, equal to E_0-E_{ex}, after exciting the autoionization state. Because the energy value, E_2, depends on the primary energy, E_0, the line spectrum due to the scattered electrons can be distinguished from that due to the ejected electrons.

The discrete line spectra due to the autoionized electrons, that is electrons ejected from autoionization states, in helium were observed by means of positive ion impact[3,4] and electron impact[1,5,6,7]. The autoionization processes in helium have been also studied by the other experimental methods. The optical absorption spectra due to the excitation of the autoionization states from ground state were measured recently by Madden and Codling[8]. The energy loss spectra of electrons scattered inelastically after exciting the autoionization states were observed by Whiddington and Priestley[9] in 1930's and measured recently by Silverman and Lassettre[10] and Simpson et al.[11,12] using the energy resolution higher than that attainable in 1930's. The several autoionization states were observed by means of the trapped-electron method which is suitable for measurement of excitation function near threshold energy[13-15].

While the energy spectra of the autoionized electrons in helium observed by 75-keV ion impact at 160° angle with respect to primary beams[3,4] showed nearly symmetric line profile, those observed by 4-keV electron impact[5] at 54° exhibited very asymmetric line profile. As in the case of the optical absorption spectra[8], the line profile of energy spectra due to autoionized electrons should contain the important informations about certain atomic parameters. Moreover, a fuller understanding of the autoionization process can be obtained from the measurements of the autoionized electrons, because the decay channel of autoionization state is designated more precisely in this kind of measurement compared with the measurement of optical absorption spectra[8]. There has been no systematic measurement on the angular distribution of the autoionized electrons.

From the general tendency of the excitation function of atoms by electron impact, the optically forbidden autoionization states can be excited intensely as the energy of primary electrons is decreased. It is especially interesting to compare the spectra of autoionized electrons by electron impact with those by molecular ion impact[3,4], particularly for the triplet-state excitation e.g., $(2s2p)^3P$. A transition from the ground state (with spin zero) to the triplet state (with spin 1) can only be accomplished by interchanging an electron from an impinging particle with one of the orbital electrons of helium. For molecular-ion impact, for instance, a molecular-hydrogen ion H_2^+ can excite that state but a proton can not, whereas

an impinging electron itself can exchange with one of the bound electrons when the impact energy is close to the excitation energy of the triplet state. The most important difference between the H_2^+ impact and the electron-impact excitations is that a bound electron of H_2^+ contributing to the exchange collision has a momentum distribution and this characteristic should be observed in the energy spectra of ejected electrons.

The energy spectra of the autoionized electrons in helium are measured in the present study as a function of ejection angle at a fixed energy of primary electrons and as a function of primary energy at a fixed angle, and some of these experimental results are analyzed by Fano's configuration interaction theory[16,17]. The line shapes of energy spectra due to the autoionization process are determined by the interference between the autoionization states and continuum states, as pointed by Fano[16]. Therfore, knowledges on electrons resulting from the direct ionization are necessary in order to understand the behaviour of autoionized electrons. The experimental results on the energy and angular distribution of secondary electrons resulting from direct ionization will be described in the following paper[18] together with the theoretical analysis.

2. Experimental Apparatus

A) Gneral description

A schematic diagram of the apparatus for the measurement of energy and angular distribution of the secondary electron ejected or scattered from gases by electron bombardment is shown in Fig. 3[19]. The electron beam with the definite energy from the electron gun is injected into the collision chamber, and monitored with the Faraday Cage. The electrons ejected or scattered from the target gas atoms are analyzed by the 90° cylindrical electrostatic energy analyzer and are focused onto the electron multiplier. The electron energy analyzer system can be rotated with respect to the primary beam over the angular range from −90° to +140°. An individual electron is counted and registered in a 400 channel scaler.

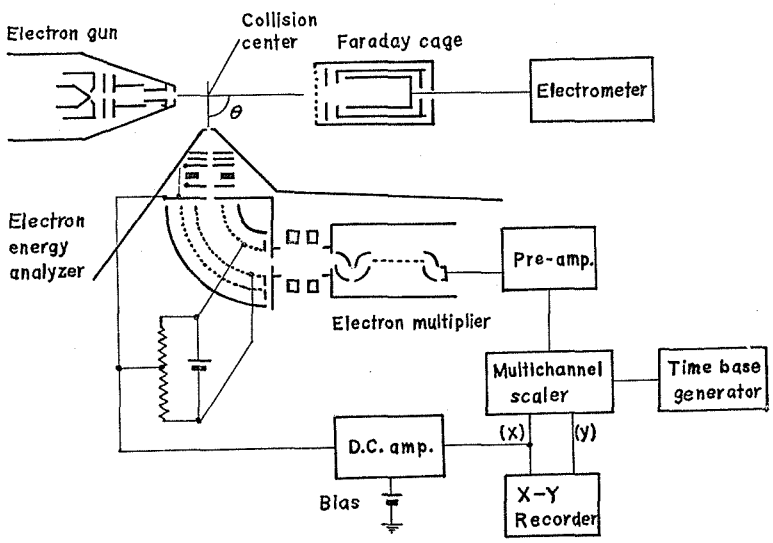

Fig. 3. Schematic diagram of the experimental arrangement.

B) Vacuum system

A cross sectional view of the scattering chamber is shown in Fig. 4. The section is that of a plane perpendicular to the plane of rotation through the electron beam path with the energy analyzer set at 0°. The system is subdivided into three regions: electron gun room A; target gas room B; electron analyzer room C. These regions are separately pumped by three independent diffusion pump systems with the molecular sheaves trap. The main part of the vacuum system is made from type 304 stainless steel, and sealed by the alminum foil or gold ring. When the vacuum system is baked out at about 200°C, the base pressure 3×10^{-9} Torr can be attained. After the electron analyzer system is set at a required angle, the target gas room is separated from both the gun room and the analyzer room. Target gas is fed into the target room from the gas reservoir through a pipe with a Granville-Phillips leak valve and is differentially pumped across the apertures. When the pressure in the target room, B, is 2×10^{-3} Torr, the pressure in the gun room and in the analyzer room is about 2×10^{-5} Torr. Target gas is purified through the molecular sheaves cooled with liquid nitrogen. The purity of the gas was verified by a guadrupole residual gas analyzer (EAI Quad 150 A). Target gas pressure was$\sim1\times10^{-3}$ Torr.

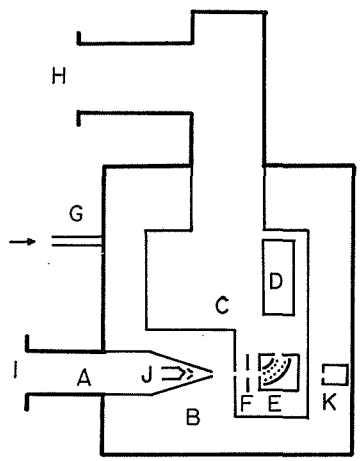

Fig. 4. Vertical cross section of experimental Apparatus.
A. electron gun room, B. target gas room, C. electron analyzer room, D. electron multiplier, E. electron analyzer, F. retarding electrode, G. target gas inlet, H and I. to diffusion pump, J. electron gun, K. Faraday cage.

C) Primary electron beam

The electron gun consisting of the tungsten filament cathode (hair-pin shape) and the cylindrical lens system is set in the gun room. The energy of the primary beam is varied from 60-eV to 1000-eV and the beam current is 20–100 μA. The energy spread of the primary beam is 0.6-eV in FWHM, estimated from the energy spectrum of electrons elastically scattered by helium gas. As mentioned in 1, the energy of electrons ejected from autoionization state does not depend on the energy of the primary beam. Therefore, the abovementioned energy spread of the primary beam has no effect on the measurement of sharp line spectra.

D) Electron energy analyzer

After the ionizing collisions, the secondary electrons are selected in a narrow angular

range by two defining slits in the analyzer system, decelerated to a constant energy (10 eV–30 eV) by varing the retarding field, F, and injected into the cylindrical electrode. The radii of the cylindrical electrodes of the analyzer are 22 mm and 28 mm. The widths of the entrance slit and exit slit of the analyzer are varied from 0.1 mm to 0.4 mm according to a required energy resolution. In order to prevent the so-called unwanted electrons which cause the background counts and distrub the electric field by increasing the space charge, the inner and outer electrodes are made by stringing 0.05 mmϕ tungsten wire just like a bamboo blind on the frames. The unwanted electron is collected by the collector which is set outside the inner and outer electrode. All electrode and grids are gold-plated to minimize the local variation of the surface potential.

E) Magnetic shielding

The residual magnetic field in the main part of the apparatus, which has an important effect upon the low energy electrons, is reduced below about 5 mG with Helmholtz coils and permalloy shields. Every part which is made from type 304 and type 316 stainless steels is thermally annealed in the hydrogen atomosphere to eliminate the induced magnetization produced by the machining. Measurements of the magnetic fields were done with a magnetic flux meter with a sensitivity of 0.02 mG.

F) Electron counting system

The energy-selected electrons are detected by the electron multiplier. The output pulses are amplified up to a required level by a charge sensitive preamplifier and amplifier, and stored in the 400 channel multiscaler. The block diagram of electronics for the electron counting is shown in Fig. 3. The retarding voltage which is applied to the retarding electrode (F, in Fig. 4) of the analyzer is generated by converting the channel adress of the multiscaler to the analog voltage by the use of the A–D converter. Thus, the channel advance of the multiscaler is synchronized with the retarding voltage within an accuracy of 0.01–eV.

3. Experimental procedure

The energy of secondary electrons was measured by the electrostatic energy analyzer mentioned in section 2 (D) in retardation mode. The electrons incident on the energy analyzer are decelerated with the retardation lens to a fixed energy and injected into the cylindrical electrodes. The energy of secondary electrons, E_{kin}, is given by

$$E_{kin}=V_r+fV_d\,, \tag{3}$$

where V_r is the retardation voltage, V_d is the potential difference between the inner and the outer cylindrical electrodes, and f is the analyzer constant determined from the radii of cylindrical electrodes. The energy, E_{kin}, derived from the measurement of V_r is often different from the true value, because of: (1) energy shift due to the contact potential, and (2) electric potential caused from space charge in the collision space. Therefore, the energy spectra measured as a function of V_r must be calibrated in the energy scale. The energy difference between two Auger peaks $M_4N_1N_{2,3}$ and $M_5N_1N_{2,3}$ in krypton, which were measured in an auxiliary run, was compared with the energy difference obtained from optical data[20]. The energy differences obtained by the present energy analyzer were in good agreement with the optical data[20] within an accuracy of 0.01–eV. Thus, the energy difference between two different positions of energy spectra can be measured within this accuracy. In order to calibrate the energy scale absolutely, the 60. 130–eV value for the $(2s2p)^1P$ level measured by Madden and Codling[8] was used to calibrate one point of the energy scale.

Refering to the peak due to $(2s2p)^1P$ state shown in Fig. 11 (section 4) for 250–eV electron impact, the full width at half-height of this peak is equal to 0.12–eV. Because the $(2s2p)^1P$ state in helium has a natural line width of about 0.04–eV, the resolving power proper to the energy analyzer is estimated to be 0.12−0.04=0.08–eV in FWHM, which is nearly consistent with the value expected. The measurements of the energy spectra over the wide energy range of secondary electrons were performed with an energy resolution of 0.15–eV in FWHM, whereas the details of the spectra within narrow energy range were measured with better resolution, i.e 0.08–eV in FWHM.

When the collision chamber is evacuated, background counts are negligibly few except the neghborhood of the forward direction. The experimental results in the directions below 10 degree were corrected for background counts. Before each set of measurements, the position of zero angle is found by determining the positions of equal current on either side of the incident electron beam, and by measuring the electron elastically scattered from the target gas on either side with respect to electron beam. Except for the angle larger than 90°, the electrons are measured at both $+\theta$ and $-\theta$ to confirm the symmetry of the both side. The angular position can be determined absolutely within an accuracy ~1° and relatively within an accuracy ~0.5°. The angular resolution of the detector system is~2 degree.

4. Results and Discussion

4–1 The energies of the autoionization states

As typical examples, the energy spectra of secondary electrons, which contain the sharp

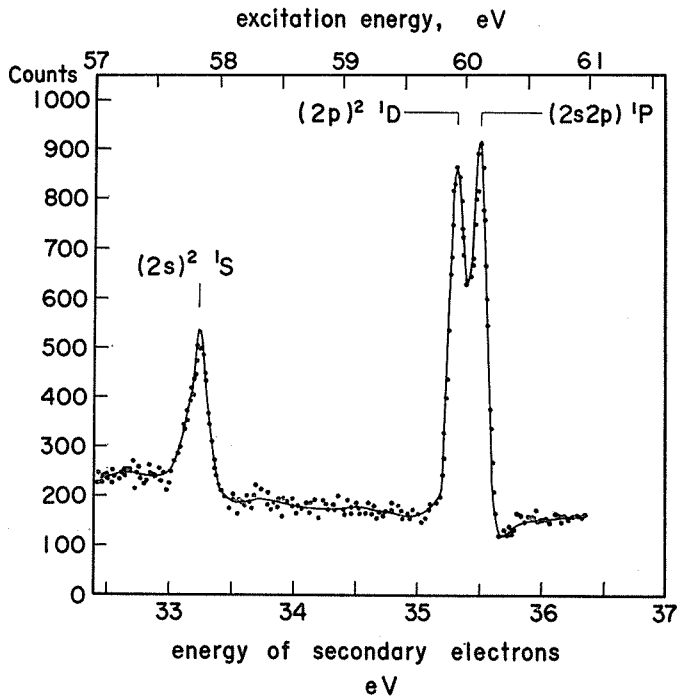

Fig. 5. Energy spectrum of autoionized electrons in helium. Primary electron energy is 180 eV and detection angle is 142°. The excitation energy of autoionization state is shown on this figure together with the energy of secondary electrons.

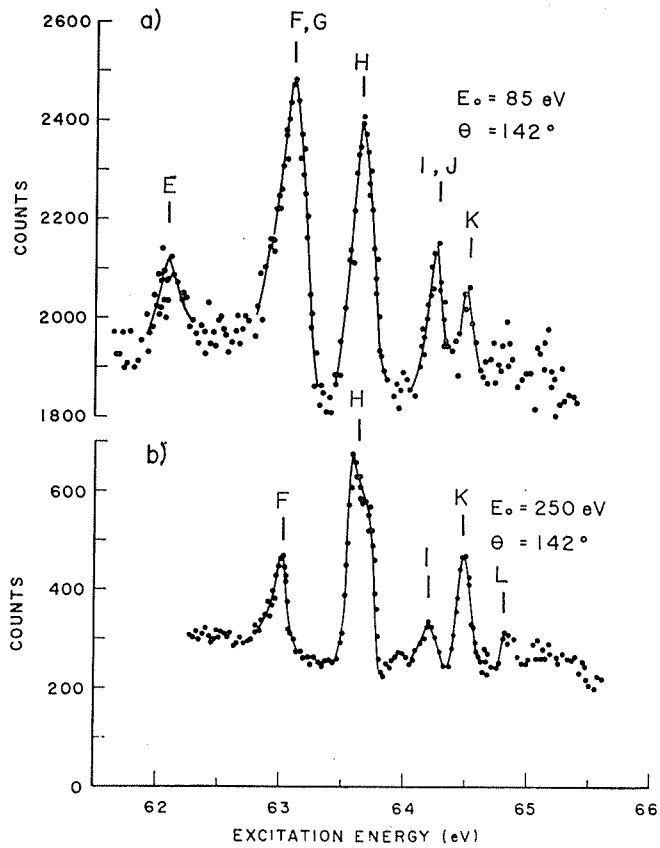

Fig. 6. As in Fig. 5 except that the enery region of autoionized electrons is higher than that for Fig. 5 and that the primary electron energy is 85 eV in (a), 250 eV in (b). In this and following figures, the autoionization states are represented by capital letters as follows:
A. $(2s^2)^1S$, B. $(2s2p)^3P$, C. $(2p^2)^1D$, D. $(2s2p)^1P$, E. $(2p^2)^1S$, F. $(2s3s)^1S$, G. $(23sp+)^3P$, H. $(23sp+)^1P$, I. $(2s4s)^1S$, J. $(24sp+)^3P$, K. $(24sp+)^1P$, L. $(25sp+)^1P$.

line spectra due to electrons ejected from autoionization states in helium are shown in Figs. 5 and 6. In Fig. 5, the energy of primary electrons is 180-eV and the energy range of secondary electrons is relating to the several autoionization states of lower energy. In Fig. 6, the energy of the primary electrons is 85-eV in (a) and 250-eV in (b), covering the higher energy regions converging to the energy of He^+ (n=2). The energy spectra shown in Figs. 5 and 6 were observed at an angle of 142° with respect to the direction of primary electrons and with an energy resolution of 0.08-eV in FWHM.

The energy differences between several peaks in Figs. 5 and 6 were determined and compared with those obtained by other experimental and theoretical methods. Some of structures seen in Figs. 5 and 6 were identified to the autoionization states by this comparison. The selection rules for an autoionizing transition from an initial excited state to a final continuum state, i.e. $\Delta L=\Delta S=\Delta J=\Delta \Pi=0$ in the LS coupling scheme, are useful for identifying the energy spectra. For instance, the structure near the peak due to $(2s2p)^1P$ is assigned to be due to $(2p^2)^1D$ state, because $(2p^2)^3P$ must be rejected because of the selection

rule. The energy values at the peaks, which were observed in the backward direction, are summarized in the second column of Table 1. The excitation energies of autoionization states measured by other groups and those calculated theoretically are shown in the other columns of Table 1.

Table 1. Excitation energy (eV) of autoionization states in helium.

	Autoionizaion State	This Paper	exp. M.C[a]	exp. Rudd[b]	exp. S.M.C[c]	exp. others	theory B.T[d]	theory B.M[e]	theory others
A	$(2S^2)^1S$	57.84		57.82	57.9	57.82[f] 57.95[g] 57.83[h]		57.865	
B	$(2s2p)^3P$	58.30		58.34	58.5	58.29[h]	58.30	58.36	
C	$(2p^2)^1D$	59.92		60.0	60.0	59.95[i] 59.86[g] 59.92[h]			60.115[l] 60.025[m]
D	$(2s2p)^1p$	60.13 (M.C)	60.130		60.1	60.0[j] 60.0[k]	60.143	60.269	
E	$(2p^2)^1S$	62.0		62.15				62.81	62.16[o] 62.13[n]
F	$(2s3s)^1S$	63.0		62.95		62.94[g]		63.01	62.97[n] 62.96[o]
G	$(23sp+)^3P$	63.0		63.08					
H	$(23sp+)^1P$	63.63	63.653		63.6	63.5[j]	63.677 63.65[g]	63.69	
I	$(2s4s)^1S$	64.2		64.22		64.22[g]		64.22	
J	$(24sp+)^3P$	64.2		64.22					
K	$(24sp+)^1P$	64.5	64.462			64.45[g]		64.48	
L	$(25sp+)^1P$	64.8	64.813			64.81[g]		64.82	

a) ref. (8), b) refs. (3) and (4), c) ref. (11). e) ref. (22). f) ref. (13).
g) ref. (6). h) ref. (7). i) ref. (15). j) ref. (10). k) ref. (5).
l) P. L. Altick and E. N. Moore: Proc. Phys. Soc. 92 (1967) 853.
m) J. W. Cooper, S. Ormonde, C. H. Humphrey, and P. G. Burke: Proc. Phys. Soc. 91 (1967) 285.
n) P. G. Burke and A. J. Taylor: Proc. Phys. Soc. 88 (1966) 549.
o) T. F. O'Malley and S. Geltman: Phys. Rev. 137A (1964) 1344.

4–2 Dependence of the energy spectra on the energy of primary electrons.

The energy spectra of autoionized electrons in the backward directions are shown in

Figs. 7* and 8 as a function of the energies, E_0, of primary electrons. The energy spectra shown in Fig. 7 were observed at an ejection angle of 142° at an energy resolution of 0.15–eV in FWHM and involve the whole energy region of autoionization states which converge to the energy of He^+ (n=2) state. Fig. 8 shows the results with higher resolution of 0.08–eV in FWHM of the energy region near 60–eV, being observed at an angle of 127°.

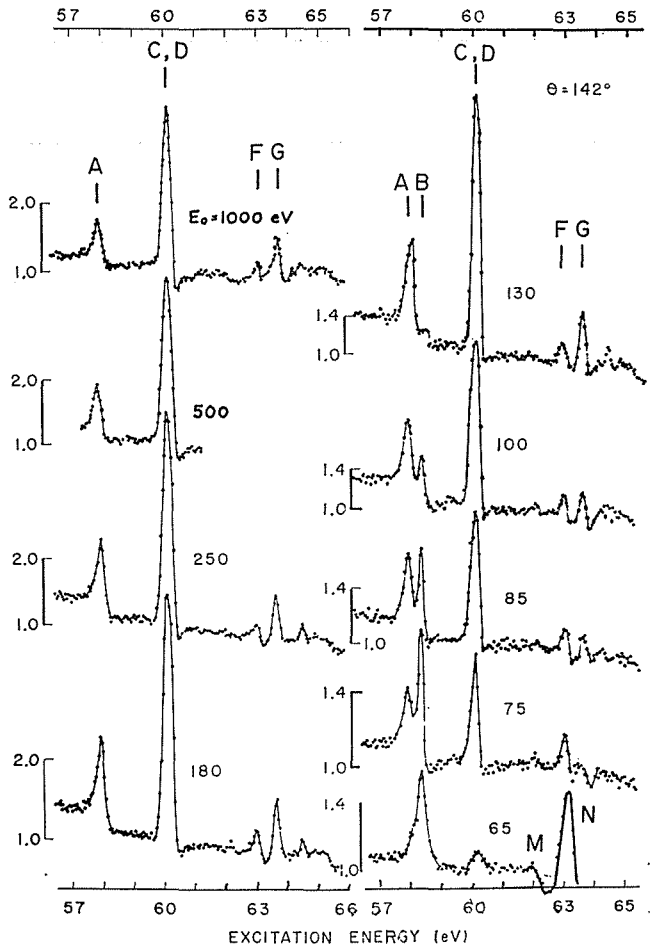

Fig. 7. Energy spectra of autoionized electrons; Dependence on the impact energy, E_0, of primary electrons; Energy resolution of electron energy analyzer is 0.15 eV in FWHM. Detection angle is 142°. The structures, M and N, are due to the electrons scattered inelastically by helium.
In this and following figures of energy spectra, the intensity scales are given as follows: the intensity of continuum at the energy of $(2s2p)^1P$ state is normalized to 1.0 and the length corresponding to the intensity scale is shown in the left-hand side of each spectrum.

* The peaks marked as M and N for E_0=65–eV in Fig. 7 are due to the electrons scattered inelastically after exciting the singly excited states, $(1sns)^{1,3}S$ or $(1snp)^{1,3}P$, in helium, because the positions of the maxima for these peaks move linearly with the energy of primary electrons.

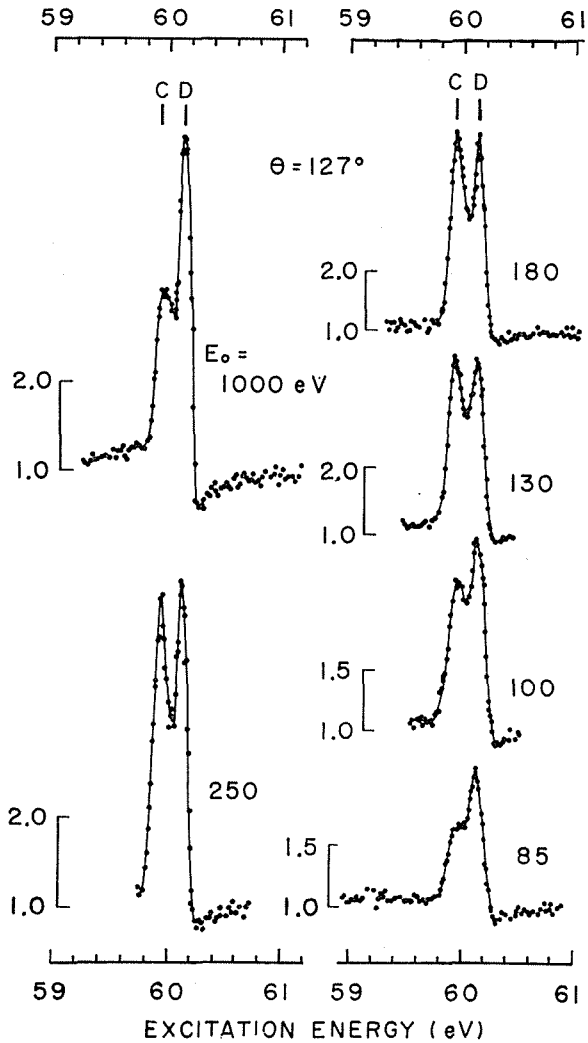

Fig. 8. Details of E_0-dependence in the neighborhood of 60-eV excitation energy. Energy resolution is 0.08-eV in FWHM. Detection angle is 127°.

The intensities in Figs. 7 and 8 are shown in arbitrary scales. In order to obtain absolute cross sections differential in energy and ejection angle of secondary electrons (hereafter, abbreviated to double differential cross section—*ddcs*), the intensity of the continuum part, $I_c(E, \theta)$, is compared with the absolute cross section, $\sigma_c(E, \theta)$, measured by Opal et al.[21]. Absolute ddcs for autoionizing lines are obtained as

$$\sigma(E, \theta) = \frac{\sigma_c(E', \theta)_{Opal}}{I_c(E', \theta)} \cdot I(E, \theta), \tag{4}$$

where $I(E, \theta)$ is the intensity of autoionizing lines obtained in the present measurement. The absolute values for *ddcs* thus obtained are reliable within an accuracy of 20–30%, taking into consideration the errors inherent in the results of Opal *et al.*[21] and those added by the present normalization procedures. The relative intensities of different energy spectra are

reliable within an accuracy of 10%. The energy spectra normalized from Fig. 7 are shown in Fig. 9 in the form of bar diagrams and resonance peak heights, *i.e.* the heights of the resonance above the local background continuum, for $(2s^2)^1S$, $(2s2p)^3P$, $(2p^2)^1D$, and $(2s2p)^1P$ states are shown in Fig. 10 as a function of the primary energy. The energy spectra of autoionized electrons in the forward directions are shown in Figs. 11 and 12 as a function of the energies of primary electrons. The detection angles are 13° and 33° for Figs. 11 and 12, respectively, and the energy resolution is 0.08–eV in FWHM for both figures. The resonance peak heights for $(2s2p)^1P$ and $(2p^2)^1D$ states are shown in Figs. 13 and 14 as a function of the primary energy. Referring to these figures, the following features are noted.

(*The energy spectra in the backward direction*; *Fig. 7–Fig. 10*)

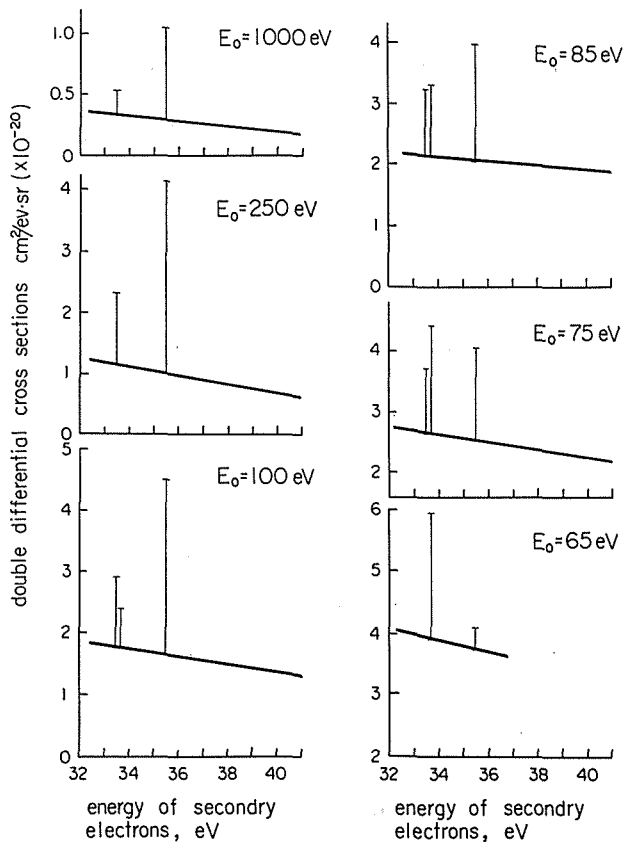

Fig. 9. The bar-diagrams of energy spectra normalized from Fig. 7 The normalization procedure is described in 4–2. The continuum parts of energy spectra are approximated by the linear lines, while the discrete energy spectra are represented by the bars which are proportional to the resonance peak height of line spectra.

(1) The resonance peak height for $(2s2p)^3P$ state is most prominent when the energy of primary electrons approaches to the excitation energy of this state (58.3–eV), and decreases rapidly with the increase of primary energy. This trend is consistent with the general shape of the excitation function for the triplet state.

(2) The resonance peak heights for $(2s2p)^1P$, $(2s^2)^1S$, and $(2p^2)^1D$ show the maxima in the

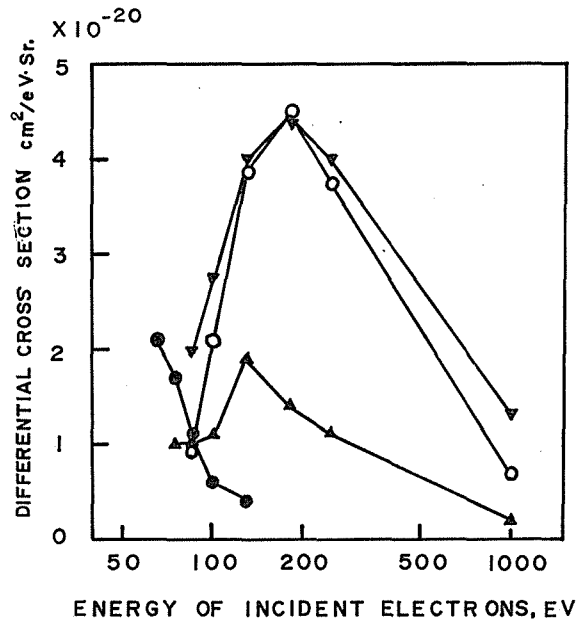

Fig. 10. E_0-dependence of the resonance peak height due to autoionized electrons in the backward directions. The resonance peak heights of the line spectra due to $(2s2p)^1P$ and $(2p^2)^1D$ were calculated from Fig. 8, while those due to $(2s2p)^3P$ and $(2s^2)^1S$ were deduced from Fig. 7. ▼–$(2s2p)^1P$, ○–$(2p)^1D$, ▲–$(2s)^1S$, ●–$(2s2p)^3P$.

regions of incident energy ranging from 100– to 200–eV. It is noted that the peaks for the optically forbidden states, $(2s^2)^1S$ and $(2p^2)^1D$, are intensely visible even at the incident energy of 1000–eV, although the ratios of resonance peak heights for the ^1D and ^1S states relative to that for $(2s2p)^1P$ state decrease as the primary energy increases above 200–eV.

(3) The line shapes of the energy spectra are nearly peak-like and remain almost invariant as the energy of the primary electrons is varied.

(*The energy spectra in the forward direction*; *Fig. 11 – Fig. 14*)

(1) As for the case of the backward direction, the resonance peak heights for $(2p^2)^1D$ state and $(2s2p)^1P$ state become maximum near the primary energy of 150–eV.

(2) The peaks for $(2p^2)^1D$ state are almost completely separated from those for $(2s2p)^1P$ state. The difference in energy between two peaks near 60–eV excitation energy is 0.23–eV, which is larger than that measured in the backward direction, i.e. 0.20–eV.

(3) While the line shapes for $(2p^2)^1D$ and $(2s2p)^1P$ state are almost peak-like in most of energy spectra, those for $(2s^2)^1S$ state change from dip-like shape to peak-like shape as the primary energy is decreased.

(4) The peak due to $(2s2p)^3P$ state becomes most prominent at the impact energy close to the threshold energy.

4–3 Dependence of the energy spectra on the detection angle.

The energy spectra of autoionized electrons by 1000–eV electron impact are shown in Figs. 15 and 16 as a function of the detection angle. The energy spectra shown in Fig. 15 were observed with an energy resolution of 0.15–eV in FWHM and involve the whole energy region of autoionization states which converge to the energy of $He^+(n=2)$ state. Fig. 16 shows the results of a more detail investigation at higher resolution of 0.08–eV in FWHM

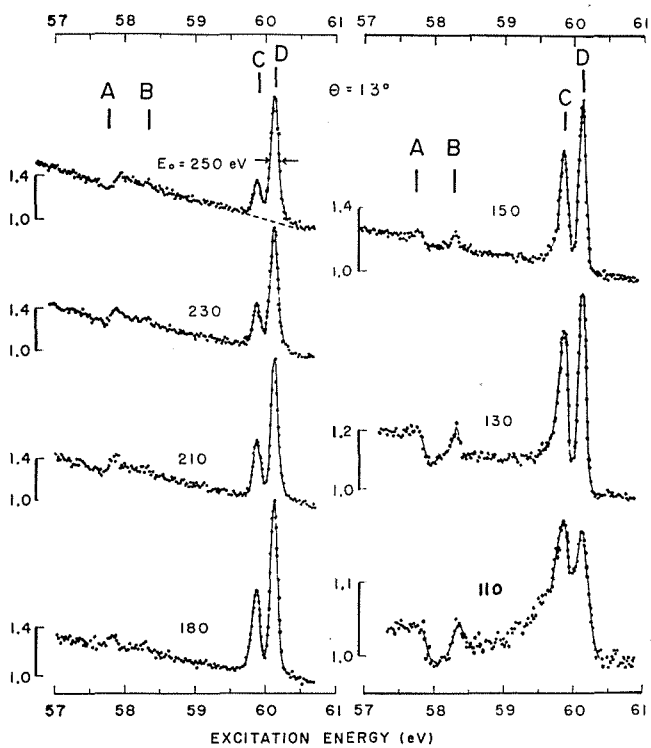

Fig. 11. Energy spectra of autoionized electrons: Dependence on the impact energy, E_0, of primary electrons; Detection angle is 13°; Energy resolution of electron energy analyzer is 0.08-eV in FWHM, which has been determined from the half width of peak, D.

of the energy region near 60-eV. The energy spectra normalized from Fig. 15 by the procedure mentioned in previous section are shown in Fig. 17 in the form of bar diagrams. The angular dependences of energy spectra due to autoionized electrons ejected by electron impact with energies of 250- , 180- , and 85-eV are shown from Fig. 18 to Fig. 23. The most prominent feature seen in these results is that the line shape of energy spectra undergoes a marked change with detection angle.

The principal features of the observed angular distributions are as follows:

(*1000-eV electron impact*: *Fig. 15*; $\Delta E_{1/2}$=*0.15-eV*, *Fig. 16*: $\Delta E_{1/2}$=*0.08-eV*, *and Fig. 17*)

(1) At smaller angles, dips are seen in both sides of a single peak in the excitation energy region near 60-eV. As the detection angle is increased, a dip on the low-energy side once disappears and another peak appears at the almost same position as that of dip in the more backward directions. It was confirmed from an auxiliary experiment utilizing the helium gas mixed with krypton gas, the position of the peak on the high-energy side remains unchanged over the whole range of angles. Therefore, peaks and dips on the high-energy side near 60-eV are identified to the same state, namely $(2s2p)^1P$ state, whercas the structures on the low-energy side are due to $(2p^2)^1D$ state.

(2) The structure of the energy spectra due to $(2s^2)^1S$ state is dip-like and very weak in the forward and intermediate angular range. In the backward directions, $(2s^2)^1S$ state becomes more prominent and exhibits the peak-like line shape.

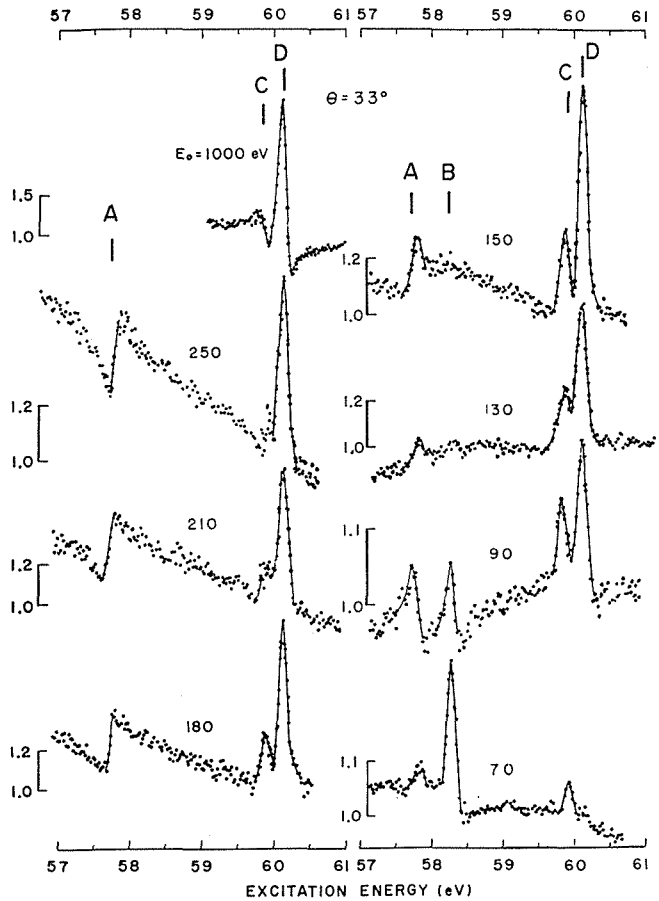

Fig. 12. As in Fig. 11 except that detection angle is 33°.

(3) The differences between ddcs at peak and that at dip for $(2s2p)^1P$ state are almost isotropic over the whole range of angles.

(*250-eV electron impact*: *Fig. 18*; $\Delta E_{1/2}$=*0.15-eV, and Fig. 19*)

(1) The line shape of the energy spectra due to $(2s^2)^1S$ state undergoes a systematic change from dip-like to peak-like shape as the detection angle is increased.

(2) The differences between ddcs at peak and that at dip for $(2s2p)^1P$ state are increased with increasing angle.

(*180-eV electron impact*: *Fig. 20*; $\Delta E_{1/2}$=*0.08-eV*)

(1) The dips on the high energy side of the peaks due to $(2s2p)^1P$ state are prominent in the intermediate angular range and become less marked both in the forward and backward directions.

(2) The spectra due to $(2p^2)^1D$ state show the peak-like line shape in the forward directions and the net peak heights relative to those due to $(2s2p)^1P$ state decrease with increasing angle to about 38°. The structure due to $(2p^2)^1D$ state exhibits dip-like line shape once in the intermediate angular regions and again become peak-like above the angle of ~70°. The differences in energy between peak due to $(2p^2)^1D$ state and that due to $(2s2p)^1P$ state are 0.23-eV in the forward directions and 0.20-eV in the backward directions.

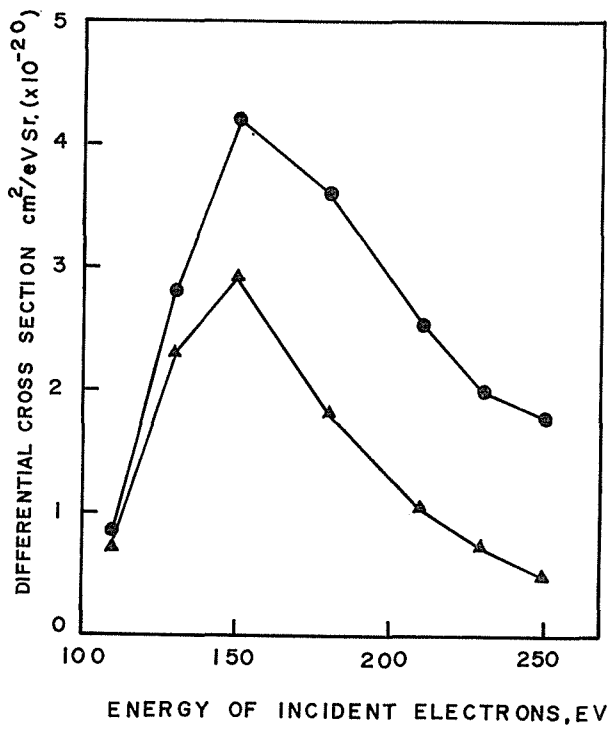

Fig. 13. E_0-dependence of the resonance peak height due to autoionized electrons in the forward directions. Detection angle is 13°. Closed circles; $(2s2p)^1P$, triangles: $(2p^2)^1D$.

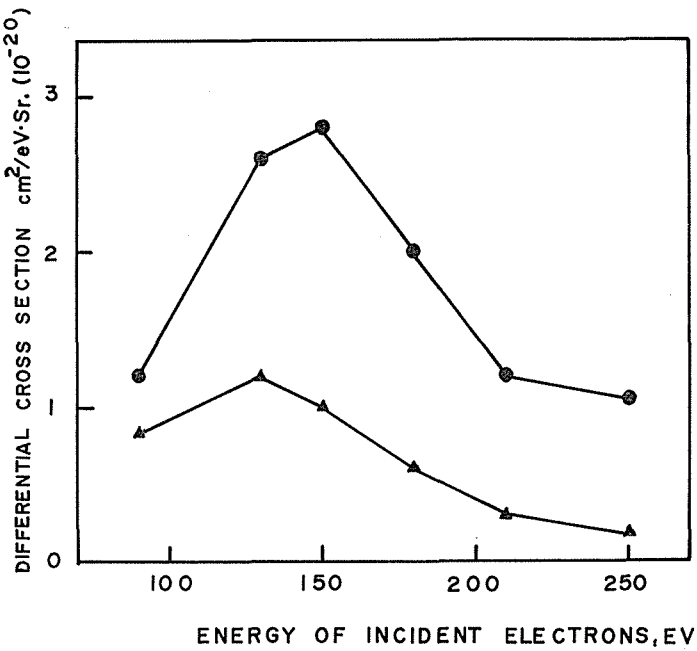

Fig. 14. As in Fig. 13 except that detection angle is 33°.

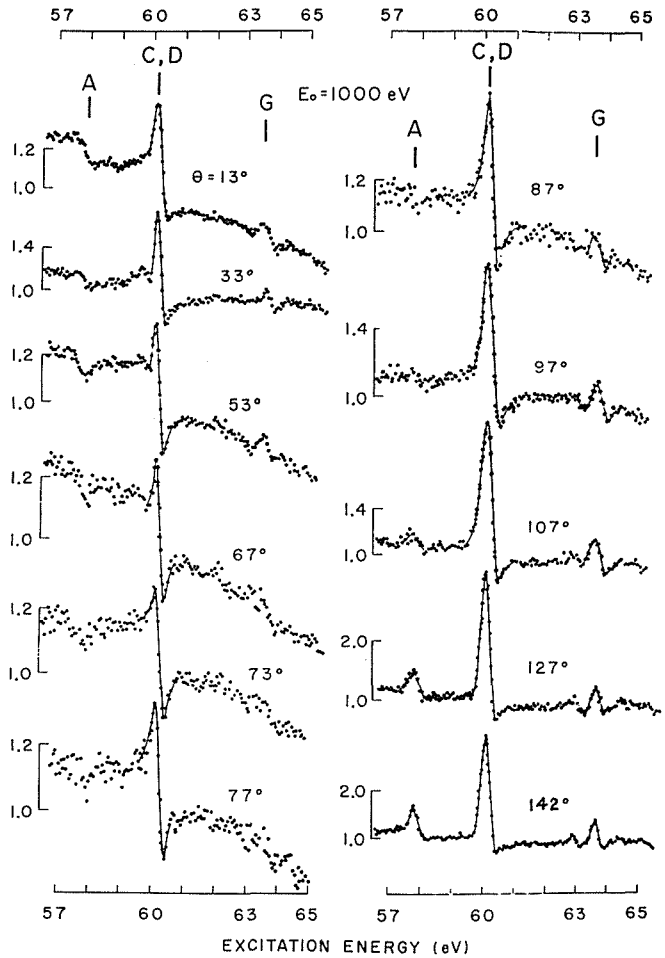

Fig. 15. Energy spectra of autoionized electrons. Primary electron energy is 1000-eV; Dependence on detection angle; Energy resolution is 0.15-eV.

(**85**-*eV electron impact*: *Fig. 21*; $\Delta E_{1/2}$=*0.15-eV*, *Fig. 22*; $\Delta E_{1/2}$=*0.08-eV*, *and Fig. 23*)

(1) The spectra due to $(2s2p)^3P$ and $(2s^2)^1S$ states are rather complicated, because these two states have the almost same excitation energy. The spectra due to $(2s^2)^1S$ have the dip-like line shape at angles below 90° and the peak-like shape above 90°. The spectra due to $(2s2p)^3P$ state are nearly peak-like over the whole range of angles. The resonance peak height due to $(2s2p)^3P$ are almost equal to that due to $(2s^2)^1S$ at 145°, decreases rapidly with decreasing angle to 100°, and again becomes visible at angles below 90°.

(2) The line shapes due to $(2s2p)^1P$ are peak-like at the almost whole angles except at 50° and 70°, where dips on the high energy side of peaks are remarkable. The resonance peak heights due to $(2s2p)^1P$ state have minimum around 100°.

(3) The differences in energy between peak due to $(2s2p)^1P$ state and that due to $(2p^2)^1D$ vary with the detection angle in complicated manner. The maximum value for this difference is 0.28-eV at 40°, and two peaks approach each other to become unable to resolve these two peaks at several angles.

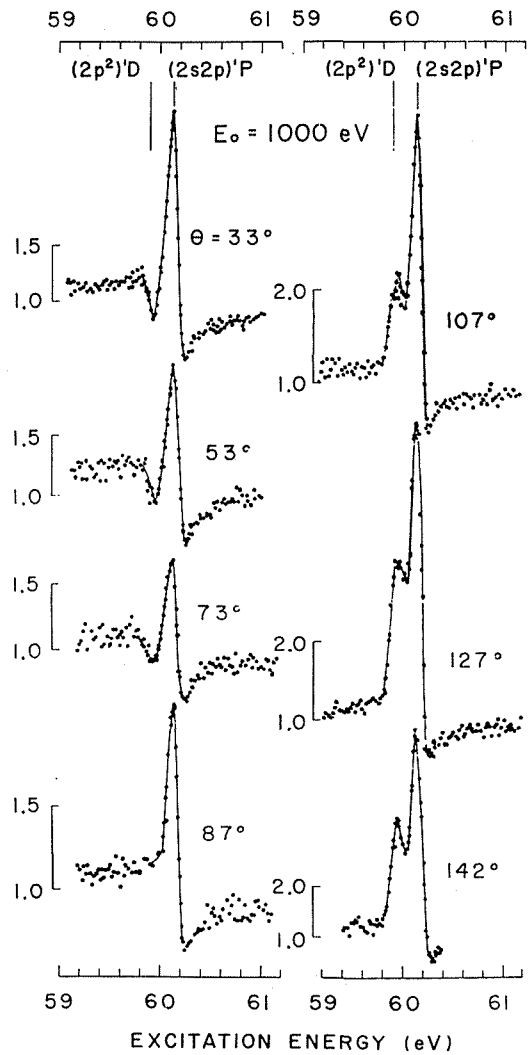

Fig. 16. Details of dependence on detection angle near 60-eV excitation energy. Primary electron energy is 1000-eV. Energy resolution is 0.08-eV.

4-4 The analysis of resonance profiles.

As in the case of resonance scattering, the line profiles of energy spectra due to electrons ejected from autoionization states should give a key to further understanding of physical processes in the present experiments. Moreover, when the line profile is quite asymmetric, the true resonance energy of autoionization state can be determined only through the analysis of line profiles, as in the case of the optical absorption spectra*.

* The energy at the maximum of peak is not necessarily the true resonance energy. For instance, the difference in energy between the peak of $(2p^2)^1D$ and that of $(2s2p)^1P$ is 0.23-eV for the forward direction and 0.20-eV for the backward direction as shown in Fig. 20. This fact shows that the position of peak depends on the line shape.

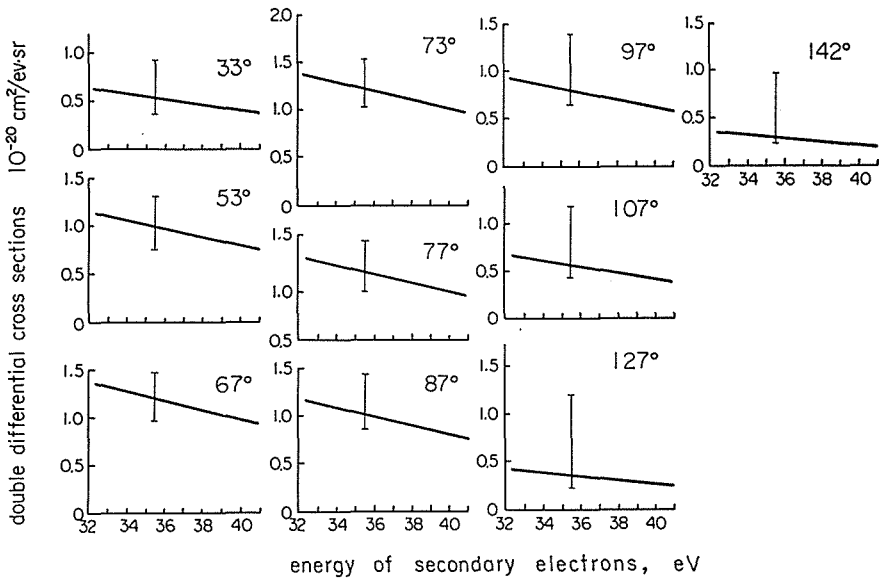

Fig. 17. The bar-diagrams of energy spectra normalized from Fig. 15. The continuum parts of spectra are approximated by the linear lines, while the discrete spectra are represented by the bars.

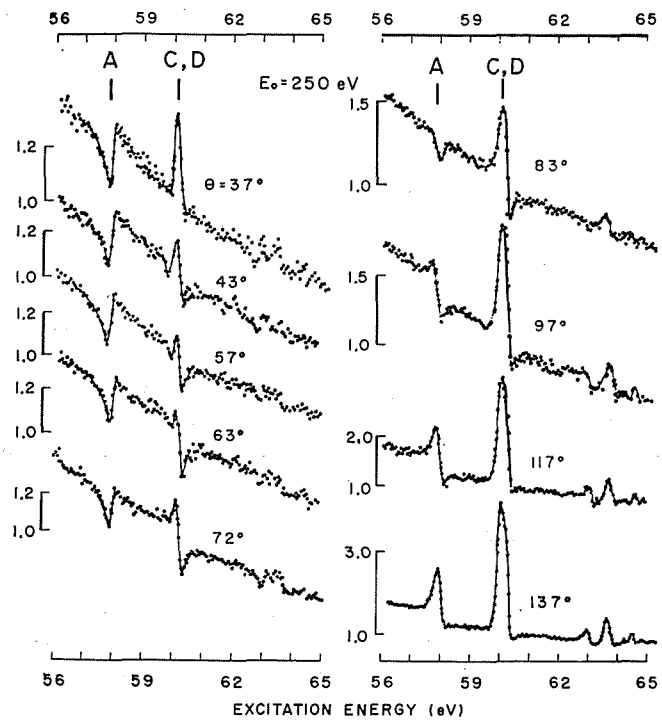

Fig. 18. As in Fig. 15 except that primary electron energy is 250-eV.

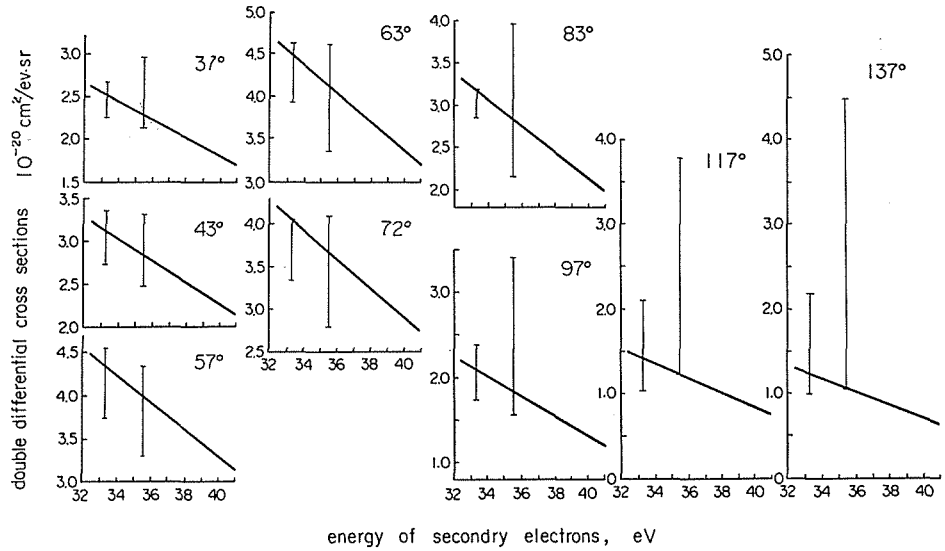

Fig. 19. As in Fig. 17 except that the original spectra are shown in Fig. 18 (E_0=250 eV)

In this section, the measured energy spectra of autoionized electrons are analyzed utilizing Fano's configuration interaction theory[16,17] and the applicability of Fano's theory is discussed.

(A) Theory

The expected profile of resonances in the photoionization continua of atoms due to the interference of autoionization states with the continua has been formulated by Fano and Cooper[16,17] as follows:

$$\sigma(\varepsilon)=\sigma_a\left[\frac{(q+\varepsilon)^2}{1+\varepsilon^2}\right]+\sigma_b \ . \tag{5}$$

Here,

$$\varepsilon=\frac{E-E_r}{1/2\Gamma} \tag{6}$$

indicates the departure of the photon energy, E, from an idealized resonance energy, E_r, which pertains to a discrete autoionization level of the atom. Also, $\sigma(\varepsilon)$ represents the absorption cross section for photons of energy E, whereas σ_a and σ_b represent two portions of the cross section corresponding, respectively, to transitions to states of the continuum that do and do not interact with the discrete autoionization state.

In eq. (5), the line profile is characterized by the parameter, q. The parameter, q, and the energy width, Γ, are expressed in terms of several matrix elements as follows:

$$q=\frac{<\varphi|T|i>}{\pi<\varphi|H|\psi_E>\cdot<\psi_E|T|i>} \tag{7}$$

$$\Gamma=2\pi|<\psi_E|H|\varphi>|^2 \tag{8}$$

where i denotes the ground state, φ denotes the autoionization state, and ψ_E denotes the continuum state which interacts with autoionization state, φ; H is the Hamiltonian of the system and T is the transition operator from the ground state, which is the dipole moment for the optically allowed transitions.

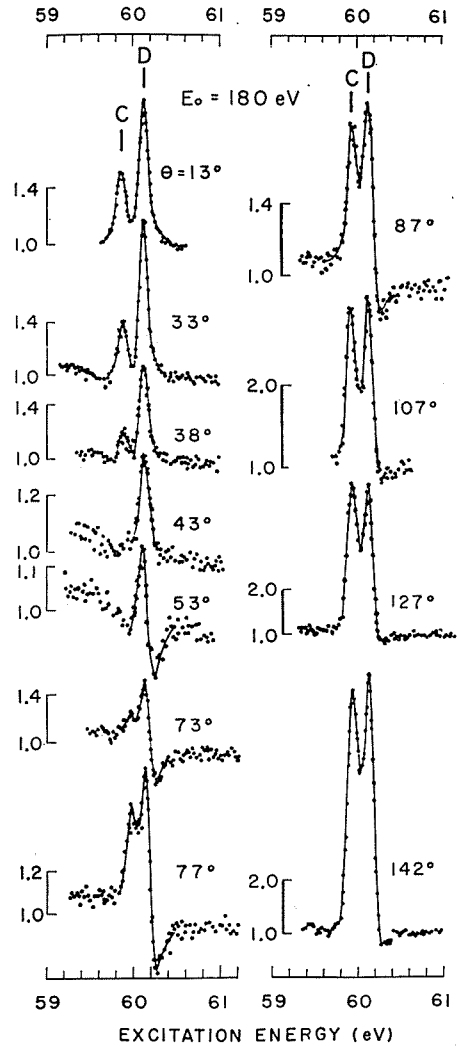

Fig. 20. As in Fig. 16 except that primary electron energy is 180 eV.

The formulation mentioned above for the case of photoabsorption spectra can be applied to the case of the energy spectra of ejected electrons by giving somewhat different meanings to the several quantities. Namely,

(1) The energy E in eq. (6) is the excitation energy derived from the energy of ejected electrons using eq. (2).

(2) The transition operator takes the form appropriate to the transition by electron impact, which makes possible a variety of transitions in addition to the dipole-allowed transition.

(3) The continuum state wave function, ψ_E, must denote not only the energy of the continuum state, but also the direction of the electrons ejected as a result of ionization.

According to these interpretations, the expression of the squared profile index, q^2, takes the following form for the case of $(2s2p)^1P$ state in helium,

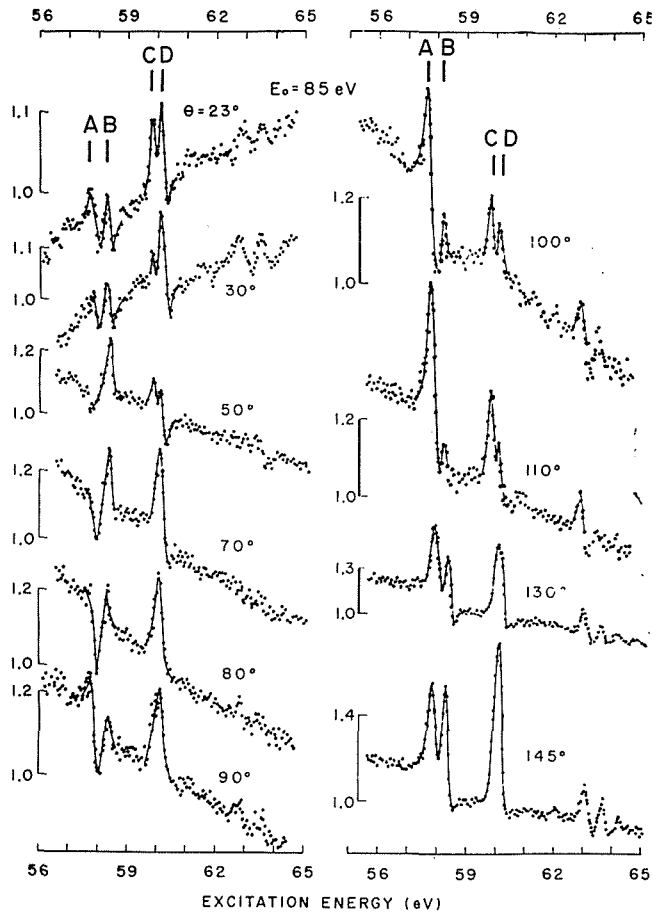

Fig. 21. As in Fig. 15 except that primary electron energy is 85–eV.

$$q^2 = \frac{|<2s2p|T|1s^2>|^2}{\frac{\Pi}{2}\Gamma \cdot |<|1sEp|T|1s^2>|^2}, \tag{9}$$

$$= \frac{\sigma_D}{\frac{\Pi}{2}\Gamma \cdot \sigma_C}, \tag{10}$$

where σ_D is the excitation cross section of the autoionization state $(2s2p)^1P$ from the ground state $(1s^2)^1S$ by electron impact, σ_C is the double differential cross section for the ejection of electrons due to the direct transition into the continuum state $(1sEp)^1P^*$ by electron impact. It must be noted that q, dimensionless quantity, is a function of the detection angle.

For the photoionization, the continuum formed in the direct ionization is $(1sEp)^1P$ state, which is the only optically allowed continuum state, whereas the other continuum

* According to the selection rules for the autoionization, the continuum state which can interact with $(2s2p)^1P$ state is only $(1sEp)^1P$ state.

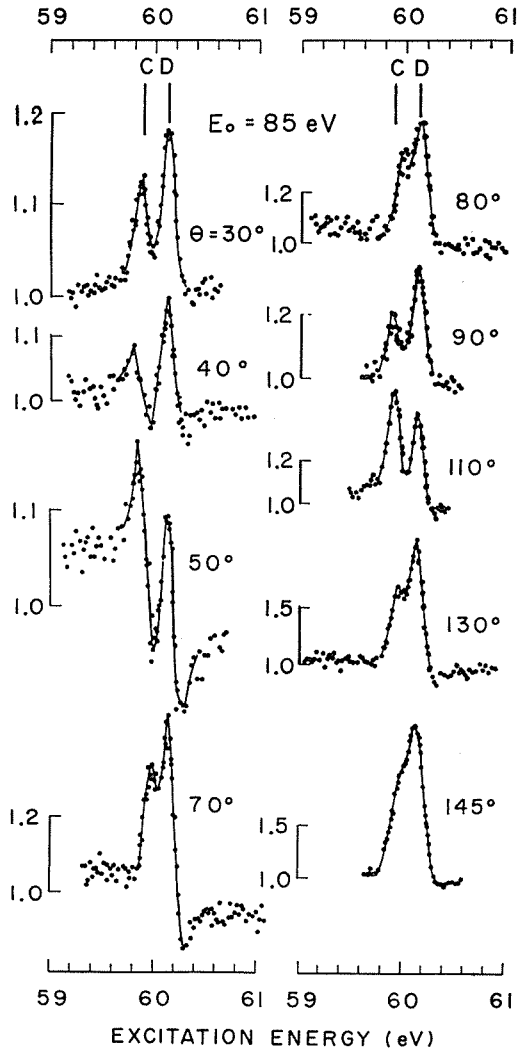

Fig. 22. As in Fig. 16 except that primary electton energy is 85–eV.

states, such as $(1sEs)^1S$ and $(1sEd)^1D$ state, can be formed in the direct ionization by electron impact, because the selection rule for the dipole transition does not hold for the transition by low energy electron impact. While the cross section, σ_b, in eq (5) is zero for the case of photo-absorption spectra in the energy region containing the autoionization states in helium converging to the energy of $He^+(n=2)$ state, σ_b for the electron impact can not be neglected, because the transitions to the continuum states that do not interact with the autoionization state are possible even in this region of excitation energy. Thus, the ratio, ρ^2 defined in the following eq. (11), becomes an important parameter which characterizes the measured energy spectra.

$$\rho^2 = \frac{\sigma_a}{\sigma_a + \sigma_b} \tag{11}$$

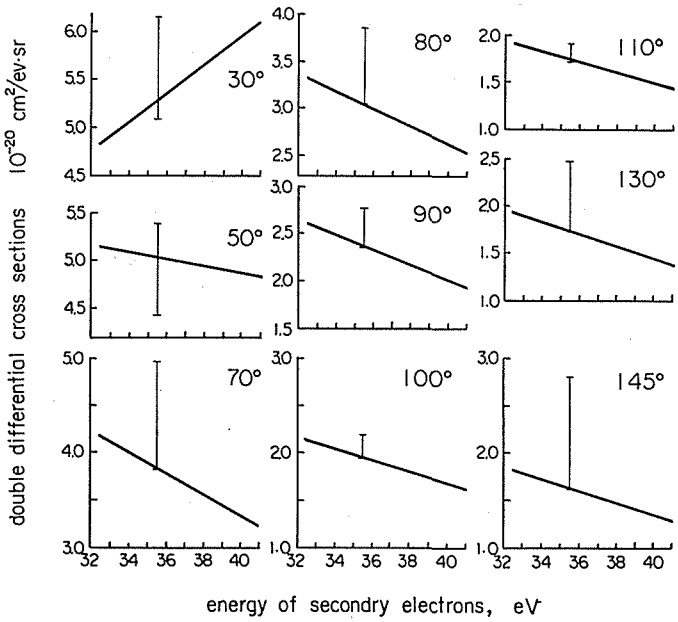

Fig. 23. As in Fig. 17 except that the original spectra are shown in Fig. 25 (E_0=85-eV).

(B) The application of Fano's theory to the measured energy spectra.

When the theoretical line shape described in (A) is applied to the measured energy spectra, several points must be taken into consideration. First, the cross section far removed from any resonance ($\varepsilon\sim\pm\infty$), which is indicated by $\sigma_a+\sigma_b$ according to eq. (5), is expressed as a linear function of the excitation energy, E, as follows:

$$\sigma_a+\sigma_b=\alpha-\beta\cdot(E-E_r)\,, \tag{12}$$

where α and β can be obtained from the observed energy spectra. By combining eq. (11) with eq. (12), σ_a and σ_b are expressed as functions of E as follows:

$$\sigma_a(E)=\rho^2[\alpha-\beta(E-E_r)]\quad, \tag{13}$$

$$\sigma_b(E)=(1-\rho^2)[\alpha-\beta(E-E_r)]\,. \tag{14}$$

Second, the line shape observed by the spectrometer is obtained by folding the line shape measured for monoenergetic electrons and the natural line shape of σ_a into the theoretical cross section.

The folded spectrum is expressed as follows:

$$y(E;q,\rho^2,E_r,\Gamma)=\int_{E-E_u}^{E+E_u}[\sigma_a(E')\frac{\left(q+\dfrac{E'-E_r}{1/2\Gamma}\right)^2}{1+\left(\dfrac{E'-E_r}{1/2\Gamma}\right)^2}+\sigma_b(E')]$$

$$\times\frac{1}{\delta\sqrt{2\pi}}\exp\left\{-\left(\frac{E'-E}{\delta\sqrt{2}}\right)^2\right\}dE'\,, \tag{15}$$

where δ is related to the full width at half-height of energy resolution, $\Delta E_{1/2}$ by $\Delta E_{1/2}=2\delta$ $(2\ln 2)^{1/2}$, and $2E_u$ is the range of the folding integration.

The least square fit of eq. (15) with parameters, E_r, Γ, q, and ρ^2, to the experimental spectra determines the values of these parameters. The following relations between Γ, ρ^2, and q is useful to estimate the rough values for these parameters,

$$\int dE[\sigma(\varepsilon)-\sigma_a-\sigma_b]=\sigma_a\cdot\frac{1}{2}\Pi\cdot\Gamma\cdot(q^2-1) \quad ,$$
$$=(\sigma_a+\sigma_b)\cdot\frac{1}{2}\Pi\cdot\Gamma\cdot\rho^2\cdot(q^2-1) \quad , \qquad (16)$$

where the value of $(\sigma_a+\sigma_b)$ is that at resonance energy, *i.e.* α in eq. (12). The value of left-hand side quantity in eq. (16) is not modified by the finite energy resolution of energy analyzer and can be directly obtained from the measured energy spectrum.

In order to get an insight for more complete fitting procedure, the following calculations were performed.

(1) The application to the energy spectra of electrons ejected from $(2s2p)^1P$ state in helium by 1000-eV electron impact. The original measured spectra are given in Fig. 16. The energy spectra due to only the state, $(2s2p)^1P$, are obtained by separating the structures due to $(2p^2)^1D$ state from the measured spectra near the 60-eV region. Fig. 24 shows an example of the theoretical curve ($q=-2.71$, $\rho^2=1.0$, $E_r=60.130$-eV, $\Gamma=0.038$-eV), together with the experimental points of the 127° curve of Fig. 16. The q-value has been estimated from eq. (16), putting ρ^2 equal to 1.0, and the values obtained by the optical absorption spectra[8] were used for E_r and Γ. The squared q-values are shown in Fig. 25 as a function

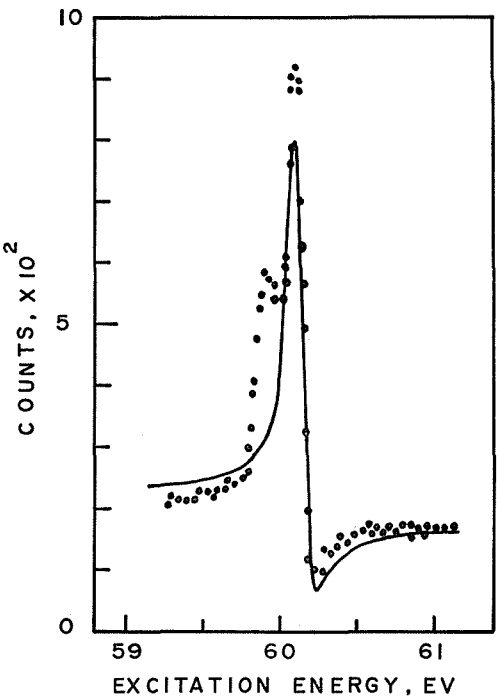

Fig. 24. An example of the line shape analysis for $(2s2p)^1P$ state in helium. Closed circles; experimental energy spectrum (Fig. 16 $E_0=1000$-eV, $\theta=127°$), full curve: theoretical line shape for $(2s2p)^1P$ corrected for finite instrumental resolving power (eq. (16)): $q=-2.7112$ and $\rho^2=1.0$.

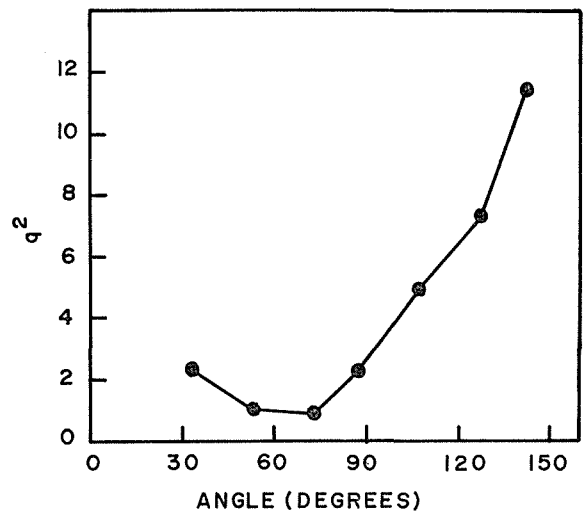

Fig. 25. The variation of q^2-value with detection angle; $(2s2p)^1P$ state in helium, $E_0=1000$–eV.

of detection angles. Because the optically allowed $(1sEp)^1P$ state occupies a large part of the continuum state formed by the direct ionization by electron impact with fairly high energy, it is reasonable to put ρ^2 value equal to 1.0. It is noted from Fig. 25 that q^2 is a function of ejection angle, as expected from the extended understanding of Fano's theory. The sign of q is negative over the whole range of angles. The true resonance energy, E_r, is derived from eq. (5) as follows:

$$E_r=E_{max}-(\Gamma/2q) \ , \tag{17}$$

where E_{max} is the position of the maximum obtained by the measurement. For instance, the energy difference between E_r and E_{max} for the 73° spectra in Fig. 25, where q is nearly -1.0, is about $0.04/(2\times1)=0.02$–eV.

(2) The application to the energy spectra of electrons ejected from $(2s^2)^1S$ state in helium by 250–eV electron impact. Fig. 26 shows the theoretical curve for the detection angle of 137°, together with experimental points from Fig. 18. The values for the resonance energy, E_r, and resonance width, were obtained from those calculated theoretically by Burke and Mcvicar[22], ($E_r=57.865$–eV, $\Gamma=0.1406$–eV), because the optical absorption spectra give no information about this state. The energy spectra due to $(2s^2)^1S$ state in this energy region of primary electrons are very suitable for the line shape analysis, because the structures due to the neighbouring states, such as $(2s2p)^3P$ state, do not yet exist in this primary energy and the natural line width for $(2s^2)^1S$ state is very wide to make minimize the effect from the resolution of the spectrometer. As shown in Fig. 26, a theoretical curve with $\rho^2=1.0$ exhibit a large departure from the experimental points, whereas that with $\rho^2=0.2$ gives a good fit. This means that the *ddcs* for the direct transition to the $(1sEs)^1S$ state at an angle of 137° by 250–eV electron impact is about 1/5 of the sum of *ddcs*'s for transition of the continuum at this angle, because ρ^2 is expressed, from eq. (11), as

$$\rho^2=\frac{\sigma(1sEs,\ ^1S)}{[\sigma(1sEs,\ ^1S)+\sigma(1sEp,\ ^1P)+\cdots\cdots]}$$

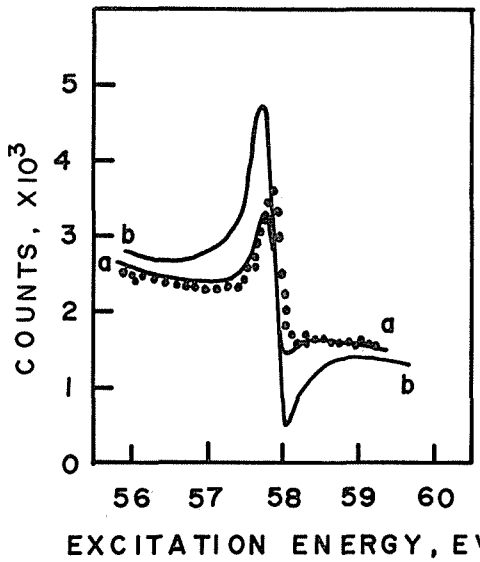

Fig. 26. An example of the line shape analysis for $(2s^2)^1S$ state in helium. Closed circles: experimental energy spectrum (Fig. 18, E_0=250-eV, θ=137°), full curve: theoretical line shape corrected for finite instrumental resolving power (eq. (16)): a) $q=-2.56$ and $\rho^2=0.2$, b) $q=-1.4525$ and $\rho^2=1.0$.

This result is reasonable, because the direct transition to the optically allowed state, $(1sEp)^1P$, occurs rather intensely for this impact energy in addition to the transition to the $(1sEs)^1S$.

ACKNOWLEDGEMENT

The author is much indebted to Professor Nobuo Oda and Mr. Fumio Nishimura of Research Laboratory of Nuclear Reactor, Tokyo Institute of Technology for many helpful suggestions and encouragement.

The experimental work described in this paper has been performed at Research Laboratory of Nuclear Reactor, Tokyo Institute of Technology by the collaboration of Professor Nobuo Oda, Mr. Fumio Nishimura, and the author. The author obtained the opportunity of taking part in this research work by the support through a grant from the Japan Society for the Promotion of Science.

He is indebted to the members of Kyoto University Data Processing Center for numerical calculations.

REFERENCES

1) N. Oda, F. Nishimura, and S. Tahira: Phys. Rev. Letters 24 (1970) 42.
2) L. J. Kieffer and G. H. Dunn: Rev. Mod. Phys. 38 (1966) 1.
3) M. E. Rudd; Phys. Rev. Letters 13. (1964) 503, and 15 (1965) 580.
4) M. E. Rudd and D. V. Lang, in Abstracts of the Fifth International Conference on the Physics of Electronic and Atomic Collisions (Science Bookcrafters, Inc., Hastings-on-Hudson, New York, 1965), p. 153.
5) W. Mehlhorn, Phys. Letters 21 (1966) 155.

6) K. Siegbahn, C. Nordling, G. Johansson, J. Hedman, P. F. Heden, K. Hemrin, V. Gelius, T. Bergmak, L. O. Werme, R. Manne, and Y. Bear, Esca Applied to Free Molecules (North-Holland Pub. Co., Amstudem, 1969).
7) H. Suzuki, M. Yamamoto, and K. Wakiya: J. Phys. Soc. Japan 28 (1970) 534.
8) R. P. Madden and K. Codling; Astrophys. J. 141 (1965) 364.
9) R. Whiddington and H. Priestley: Proc. Roy. Soc. A 145 (1935) 462.
10) S. M. Silverman and E. N. Lassetre: J. Chem. Phys. 40 (1964) 1265.
11) J. A. Simpson, S. R. Mielczarek, and J. Cooper: J. Opt. Soc. Am. 54 (1964) 269.
12) J. A. Simpson, G. E. Chumberlain, and S. R. Mielczarek: Phys. Rev. 139A (1965) 1039.
13) P. D. Burrow and G. J. Schulz: Phys. Rev. Letters 22 (1969) 1271.
14) J. T. Grissom, R. N. Compton, and W. R. Garrett: Phys. Letters 30 A (1969) 117.
15) P. D. Burrow: Phys. Rev. 2A (1970) 1774.
16) U. Fano: Phys. Rev. 124 (1961) 1866.
17) U. Fano and J. W. Copper: Phys. Rev. 137A (1965) 1364.
18) S. Tahira: To be published in Memoirs of the Faculty of Science, Kyoto University, the following paper.
19) N. Oda, F. Nishimura and S. Tahira: Bull. Tokyo Instit. Techn. 96 (1970) 27.
Details on the experimental apparatus have been given in this reference.
20) R. P. Madden and K. Codling: J. Opt. Soc. Am. 54 (1964) 268.
21) C. B. Opal, E. C. Beaty, and W. K. Peterson: Joint Institute For Laboratory Astrophysics Report; 108, univ. Colorado, Boulder, Colorado, (1971).
22) P. G. Burke and D. D. Mcvicar: Proc. Phys. Soc., 86 (1965) 989.
23) A. K. Bhatia and A. Temkin: Phys. Rev. 182 (1969) 15.